© Universiti Tun Hussein Onn Malaysia Publisher's Office

IJIE

http://penerbit.uthm.edu.my/ojs/index.php/ijie
ISSN : 2229-838X e-ISSN : 2600-7916

The International Journal of Integrated Engineering

Characterization of 3D Orthogonal Woven Carbon/Kevlar Composite Under Tensile Loading

Ram Vishal G[1*], Dalbir Singh[1], Srikanth H. V[2]

[1]School of Aeronautical Engineering,
Hindustan Institute of Technology and Science, Chennai- 603103, INDIA

[2]Aeronautical Engineering Department,
Nitte Meenakshi Institute of Technology, Bangalore- 560064, INDIA

*Corresponding Author

DOI: https://doi.org/10.30880/ijie.2023.15.05.018
Received 10 April 2023; Accepted 22 June 2023; Available online 19 October 2023

Abstract: In the present work, the tension response of polypropylene (PP) based composites reinforced with Carbon/Kevlar fabrics was investigated. The weft, wrap, and binder are considered in the direction (XYZ) and woven into a 3D fabric. Two homogeneous fabrics with Carbon (CCC), Kevlar (KKK), hybrid Carbon/Kevlar (CCK), and hybrid Kevlar/Carbon (KKC) fabrics were produced using a hand-made spoke frame. The architecture of the fabrics was three-dimensional orthogonal (3D-O). Four different composite laminates were manufactured using a vacuum bag-assisted moulding technique. The tensile loading was applied using a Nano-UTM set-up at travel of +6.25/-3.1 mm and software-automated generation of stress-strain data. The results indicated that the tensile properties of thermoplastic 3D-O composites are sensitive. In all the composites, the peak stress, strength, and modulus were increased when noticed with the 2D fabric. The experimental results show that the tensile strength of CCK and CCC with carbon fibres used in their weft and warp direction was greater than that of KKC and KKK with Kevlar fibres used in fibres weft and warp direction. The hybridization and 3D orthogonal weaving method also increased the tensile strength. The observation was characterized through scanning electron microscope.

Keywords:3D-orthogonal, hybrid, vacuum bag, tensile strength, carbon, Kevlar, thermoplastic

1. Introduction

A 3D fabric is a fabric that must be shaped to cover a thick fabric shape. In 3D knitting, weft yarns, warp yarns, and binder fibres are gathered along and through the fabric in the X, Y, and Z directions. 3D weaving is a new technology that has many advantages compared to 2D composite manufacturing. [16] Three-dimensional composites use fibres made from filaments or bundles to form a complex three-dimensional structure, instead of 2D, where the weave pattern is only on one plane. The thickness direction of a 3D fabric is called yarn, warp or wrapping yarn. At the same time, a fabric layer is woven in which several layers of warp and weft are woven from the yarn. At the end of the weaving process, an integrated 3D fabric structure with a considerable thickness is created. Woven can be used for composite materials with a fiber volume fraction of approx. 50% in 3D units and orthogonal 3D structures. Fig.1 (a,b,c), 3D woven fabrics are classified into 3D woven interlock, 3D orthogonal and 3D multilayer [17-18]. 2D-plain weave laminate; the orthogonal three-dimensional fabric is different from two-dimensional fabric in thickness; in three-dimensional fabric, Z-yarn combines warp and went into a single structure. In addition, the warp and weft threads in the 3D fabric are aligned in the 0° or 90° direction and will not be curled. [15] Three-dimensional (3D) textile preforms have been developed by using different manufacturing techniques like weaving, knitting, braiding, stitching, and non-woven manufacturing [6]. Among these manufacturing techniques, sewing and 3D weaving are promising technologies

*Corresponding author: ramvishal32@gmail.com
2023 UTHM Publisher. All rights reserved.

which address the shortcomings of stack-reinforced composites. 2D laminates and 3D composite fabrics were tested for tensile strength and flexural strength to show the mechanical superiority of 3D woven fabrics over 2D laminates.

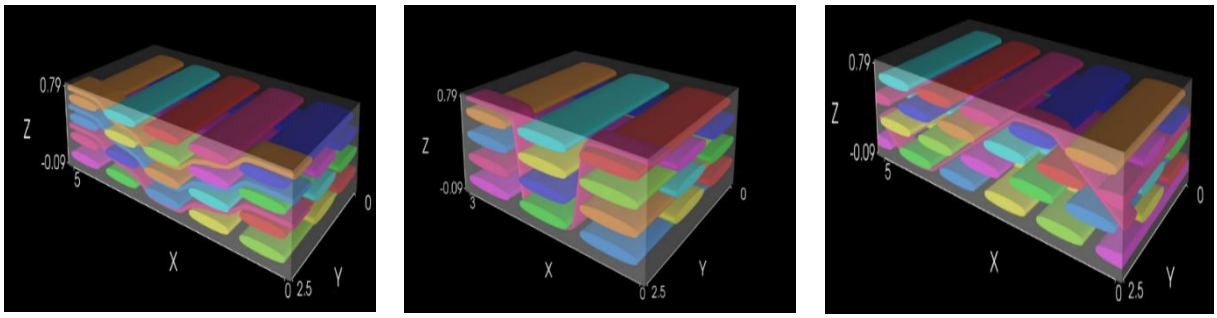

(a) (b) (c)

Fig. 1 - 3D Woven Fabrics (a) interlock; (b) orthogonal and; (c) multilayer

Nowadays many structures or parts are being made from composites and they are playing a vital role in various fields like aerospace, automobile, etc. The main reason behind the success of composite materials is because of their great characteristics. So many industries and companies are busy manufacturing composite materials, and, on another hand, many researchers and scientists are constructing composites and performing various experiments to find and study their properties at both micro and macro level. By knowing all those properties related to every composite, we can use them according to their strengths and applications. There are various methods to fabricate composites but mostly used is 3D woven composites. Enhanced properties and very flexibility for a wide range of applications are key to the success of 3D woven composites. Many studies had been carried out by various researchers and many papers had been published on 3D composites some of them are presented below with their achievements. [1]In terms of stiffness and strength, the 2/2 fabric type clearly outperforms the 1/3 fabric type along the warp and fill direction. Furthermore, the warp direction of the textile is stiffer and stronger than the filling direction for both fabric types. The agreement of Finite Element Method and experimental data demonstrates that the Finite Element Method may be utilized to characterize the mechanical properties of 3D woven fabric composites. [2] The merits, shortcomings, and different downsides have been identified. It also evaluates the, involved in bringing new technology to the industry.[3]In-depth research is done on the various procedures used in the manufacturing of 3D woven fabric preforms. Additionally, it makes a distinction between fabrics made with conventional methods and those made with special weaving equipment. Additionally, it describes the numerous varieties of woven textiles as well as the manufacturing method. Modern 3D weaving machines can create large-scale fabrics, but they are much harder to come by than conventional weaving machines.[4] After gathering the crucial strength and stiffness of the basic property data through material testing for design, the FEM model was constructed for computer analysis. To compromise on the best fiber orientations, they first established the shape, size, and orientation of the fiber for the anticipated load. The experiment used the resin transfer method. Weight reduction rates of 30% or more were achieved using 3-D composite materials for airplane construction. Additionally, 3-D composite test items were developed and put to the test, and it was determined that they met the requirements for static and fatigue strength. [7] The quasi-static three-point bending, and fatigue damage characteristics of the three-dimensional angle-interlock woven composite and the three-dimensional orthogonal woven composite were examined. Stress-deflection curves and failure modes were taken to compare the mechanical properties of both composite materials under quasi-static bending loading conditions. S-N curves were generated to compare the fatigue life under different stress levels of a three-dimensional angle-interlock woven composite with a three-dimensional orthogonal woven composite. As a result, it was established that non-crimp yarns had a considerable impact on the structural characteristics of 3D composites. [8] It was found that the overall reduction in tensile strength caused by weaving damage for dry carbon fiber yarns was 9–10%. This is far smaller than the measured 30% drop for glass fiber yarn.

It was found that the original weave's architectural design significantly affects the material's tensile mechanical strength properties. [9] In the instance of impact damage, three damage processes were observed: matrix cracking, fibre breaking, and fibre pull-out. The only technologies employed to determine these damages were NDT and CT acoustic emission (AE). The research finishes by highlighting the knowledge gap in the literature as well as the many forms of testing, such as NDT and CT, that are necessary to properly describe such material systems before depending on them in real-world applications. [10] Here, a four-step experimental method that combines digFital picture correlation, acoustic emission, and micro-XCT is suggested. Using an experimental four-step phased technique, the impact of micro cracks on the tensile characteristics of 3D woven composites is investigated. The damage mechanisms, evolution process, and residual performances were characterized using a combination of the aforementioned AE, DIC, and micro-XCT. Micro-XCT cannot detect early damage, and early damage has minimal effect on the remaining qualities. The stress varies from 65.98% to 72.93% of a second before visible internal damage occurs. The principal damage processes revealed by the CT scan are resin fractures in resin pockets, yarns, and interface de-bonding. [11] Using

modelling approaches to characterize the mechanical and impact behavior of 3D woven composites, as well as their advantages and disadvantages. ABAQUS and FEM were used to create 3D woven composite models. Detailed microstructure modelling methodologies have proven to be costly for impact assessments due to the necessity for supercomputing. [12] To establish a benchmark for all 3D composites, many experiments, including bias extension and flexural tests, were conducted. For both unbalanced and balanced shear testing at various temperatures and speeds, bias extension and trellis frame tests were employed. The outcomes of the balanced and unbalanced tests were comparable. The tensile strength was unaffected by loading speed.

2. Methodology

2.1 Materials

In the hybrid composite, the binder is woven at 45 degrees to the weft and warp (Fig. 2). We aim to bind the layers of weft and warp at an angle of 45 degrees to find out the change in its mechanical characterization. We will be using fully carbon and Kevlar as our tows. We will make four types of 3d woven composites, and they are:

(X, Y, Z): (Carbon, Carbon, Carbon): Carbon will be used as weft, warp, and binder.
(X, Y, Z): (Carbon, Carbon, Kevlar): Carbon will be used as weft, warp, and Kevlar for binder.
(X, Y, Z): (Kevlar, Kevlar, Kevlar): Kevlar will be used as weft, warp, and binder.
(X, Y, Z): (Kevlar, Kevlar, Carbon): Kevlar will be used as weft and warp and carbon as binder.

We have hand-weaved four different types of fabrics using different fibers shown in Fig.3. Different types of fabrics are as; Carbon-Carbon-Carbon: In this fabric, we have used carbon fiber as weft yarn, warp yarn and Carbon fiber as binder yarn as well, shown in Fig.3(a). Carbon-Carbon-Kevlar: In this fabric, we have used carbon fiber as weft yarn, warp yarn and Kevlar fiber as binder yarn, shown in Fig. 3(b). Kevlar- Kevlar- Kevlar: In this fabric, we have used Kevlar fiber as weft yarn, warp yarn and Kevlar fiber as binder yarn as well, shown in the Fig.3(c). Kevlar- Kevlar- Carbon: In this fabric, we have used Kevlar fiber as weft yarn, warp yarn and Carbon fiber as binder yarn, shown in the Fig.3(d). Matrix is a combination of resin and hardener. Resins are of two types and are as follows: Each resin will have a prescribed hardener to use with. In this study, Araldite LY 556 resin and HY 951 hardener were used shown in Fig.4. The property of resin is shown in Table 1. A resin-to-hardener ratio of 10:1 by weight was taken. The liquids were first poured into a container and mixed. Then the mixture was applied to the fabric uniformly. After preparation fabric was converted to a laminate by means of a vacuum bagging process. Although 3D woven weaves have very low permeability [4]proper wetting was insured by applying a matrix on both sides of the fabric. The reason for using vacuum bagging was the low cost. A vacuum pressure of 25 in of Hg was maintained and was turned on and left for 6 hours. Then the pump was disconnected and left for 48 hrs. Five specimens were made for testing the four different fabrics.

A resin to hardener ration of 10:1 by weight was taken. The liquids were first poured on a container and mixed. Then the mixture was applied on the fabric uniformly. After preparation fabric was converted to a laminate by means of a vacuum bagging process shown in Fig.5. Although 3D woven weaves have very low permeability [16] proper wetting was insured by applying a matrix on both sides of the fabric. The reason for using vacuum bagging was the low cost. Vacuum pressure of 25 in of Hg was maintained and was turned on and left for 6 hours. Then the pump was disconnected and left for 48 hrs. Five specimens were made for testing the four different fabrics.

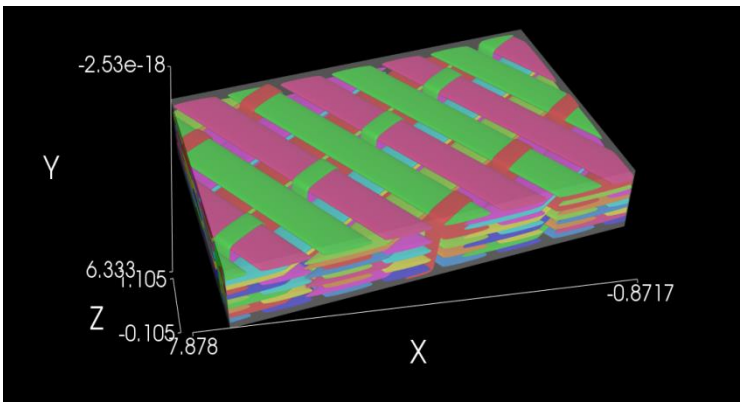

Fig. 2 - TEXGEN model of a 3D woven composite bonded at an angle

2.2 Fabrications of Specimens

Following specific ASTM testing standards, Fig.7. shows specimens were cut out from the laminate using an angle grinder. Specimens were taken in two mutually perpendicular directions. [6] For the tensile testing, D3039 ASTM standards were used i.e., 250*25 length and width as shown in Fig. 6. Specimens are subjected to a tension load until it fails. The test pieces are placed and clamped at UTM, and the tensile load is applied. Using the stress-strain data, young's modulus is calculated. The ratio of the maximum load to the specimen's area is used to compute the tensile strength.

(a) (b) (c) (d)

Fig. 3 - 3D Woven composite fabric (a) CCC; (b) CCK; (c) KKK and; (d) KKC

Table 1 - Matrix properties

Aspect	Standards	Specifications
Color	ISO 4630	Clear, pale-yellow liquid
Epoxy content	ISO 3000	5.30-5.45 [eq/kg]
Viscosity at 250 C	ISO 9371B	10000-12000[mPas]
Density at 250 C	ISO 1675	1.15-1.20 [g/cm^3]
Flash point	ISO 2719	> 2000 C
Storage temperature		2- 400 C

Fig. 4 - Resin and hardener

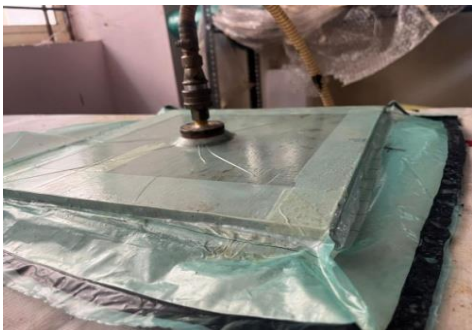

Fig. 5 - Vacuum bagging process

Table 2 - Weight of fabric, resin and hardener

No	Specimen	Fabric weight, gm	Resin weight, gm	Hardener weight, gm
1	Carbon-Carbon-Carbon	62	111.6	12.4
2	Carbon-Carbon-Kevlar	60	108	12
3	Kevlar-Kevlar-Carbon	58	104.4	11.6
4	Kevlar-Kevlar-Kevlar	55	99	11

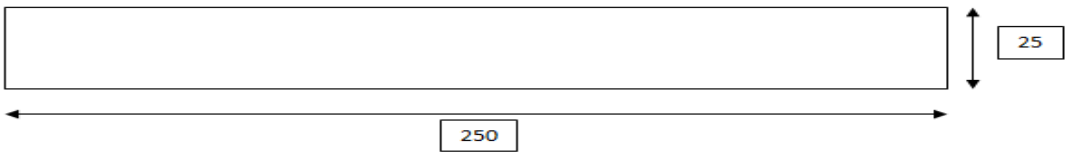

Fig. 6 - Tensile specimen ASTM-D3039

2.3 Physical Characterizations

In composite research, it is known that the maximum in-plane strength of the composite is influenced by tows in 90/00 directions, and it has little quantity of binding tows to prevent delamination. In this project Analytical solution for the determination of geometric illustration of composite RVE is dependent on the aggregation of tow in all three directions is presented. The model uses accessible data of the manufacturers as input for the further calculation of required properties. Fig.1 illustrates the type of weave pattern and contains the unit cell which is required for the calculation. [14] The model allows for the separation of the necessary dimensions of reinforcements in the X, Y, and Z axes by predicting fibre volume percentage, net thickness, and RVE density. Fig.8 illustrates a cross-section of an ellipsoid tow, which is supposed to have an elliptical form. This shape's aspect ratio (AR) is defined as AR=l/h. For a circular cross-section of tow, the aspect ratio is one (1) in which if the aspect ratio goes on increasing the flattening of the tow occurs.

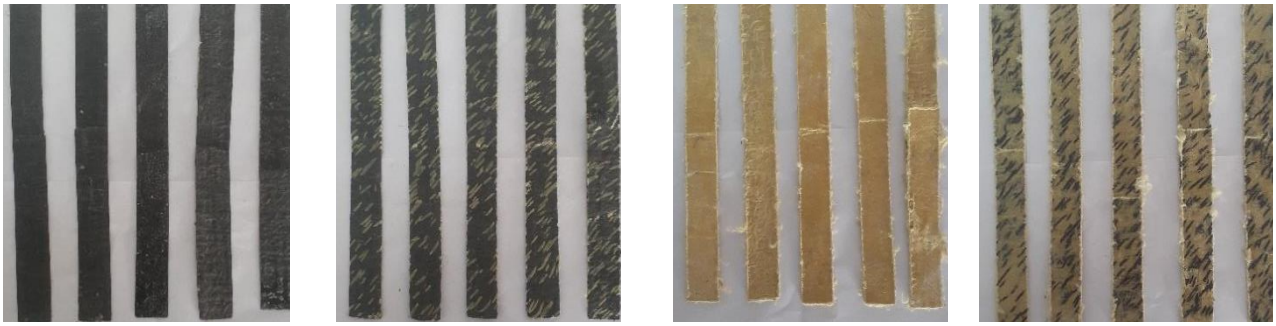

(a) (b) (c) (d)

Fig. 7 - Tensile specimens ASTM-D3039 (a) CCC; (b) CCK; (c) KKK and; (d) KKC

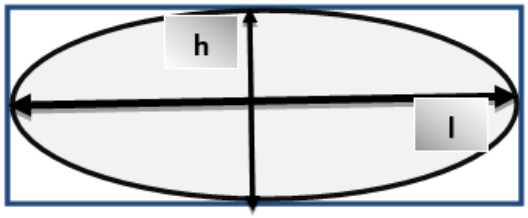

Fig. 8 - Yarn cross-section

Parameters specified by manufacturer "ρ" warp, weft and binder tow Density (kg/m3) is same in all directions (1780 kg/m3), "Y" Yield tex of weft, warp and binder tow (g/m). (0.02g/m), "Ɪ]" Stuffer, filler, and binder tow's Linear density (kg/m). Parameters specified by weaver are (ṅs, ṅf, ṅb) Number of stuffers(s) in weft (Y), fillers (f) in warp (X), binders (b) in weft (Y) in the unit cell respectively. By studying patterns of unit cells in all direction the values of ns= nf= nb=4. $\lambda_{s,f,b}$. The quantity of stuffers, binders, and fillers in the two directions per unit length (/m). The unit cell's filler, stuffer, and binder layer count is represented by $n_{s,f,b}$. From Fig.2 of side view the values of ṅs= ṅf= ṅb=4 and the values of λs=λf=5 and λb=4. Calculated parameters j = (S, f, b) where S=stuffer,f=filler,b=binder. ts, tf, tb is the j's Thickness. T is RVE Thickens. ls, lf, lb is the j's Length. Ls Lf Lb is the Net length of j's tows in RVE. Ztl is the Net length of the binder tow in RVE. Vs, Vf, Vb is the j's Net volume. The Net Volume of Reinforcement (Xtv, Ytv, Ztv) runs perpendicular to the X, Y, and Z axes. In the X and Y axes, LX, LY is the net of a unit cell. A stand for the unit cell's area. Pf is the Tow-packing factor. Vfs, Vff, Vfb is the Volume fractions j's (%). Vfx, Vfx, Vfx is the percentage of fibre volume that is parallel to X, Y, and Z directions (%). The thickness of the tow may be estimated using equation *(2)* by knowing the linear density, packing factor, and aspect ratio of the fibre, the packing factor for a rectangular packing array is assumed as 0.7854.

$$t_i = 2\sqrt{\frac{n_i}{\rho ARP_f \pi}} \tag{2}$$

where (i=s, f, b). Calculating the thickness of j tow, and the total thickness of the assumed unit cell is calculated from equation (3):

$$T = n_s t_s + n_f t_f \tag{3}$$

Equations are used to compute the length of the stuffer, filler, and binder tows as the following parameter. (4), (5), and (6):

$$l_s = \frac{\dot{n}_f}{\lambda_f} \quad (4)$$

$$l_f = \frac{\dot{n}_s}{\lambda_s} \quad (5)$$

$$l_b = \dot{n}_f h_f AR + 2H \quad (6)$$

Individual, filler binder, and stuffer tow net lengths and related tow volumes may be estimated using equations (7) and (8), respectively.

$$L_i = l_i n_i \dot{n}_i \quad (7)$$

The net volume of every single tow is,

$$V_i = L_i A_i \quad (8)$$

Where, A_i is area of cross section of each tow and calculated using equation (9)

$$A_i = \frac{n_i}{\rho P_f} \quad (9)$$

$$Z_{ti} = \dot{n}_b 2T \quad (10)$$

In the x and z axes, respectively, the vertical component of binder tows and just the horizontal component of the stuffer volume make up the tow's actual volume,

$$X_{tv} = V_s + (L_b - Z_{ti})A_b \quad (11)$$

$$Y_{tv} = V_f \quad (12)$$

$$Z_{tv} = Z_{ti} A_b \quad (13)$$

Finally, the quantities may be used to calculate the percentage of stuffer, fillers, and binder,

$$V_{fs} = \frac{V_s}{V_s + V_f + V_b} 100 \quad (14)$$

$$V_{ff} = \frac{V_f}{V_s + V_f + V_b} 100 \quad (15)$$

$$V_{fb} = \frac{V_b}{V_s + V_f + V_b} 100 \quad (16)$$

The above equation gives a measure of total RVE fiber volume engaged by each fiber in the RVE. When determining the volume % of fibre along the x, y, and z axes, the position of the binder must be taken into account. Due of the binder's involvement in both warp (X) and vertical (Z) flows:

$$V_{fx} = \frac{X_{tv}}{X_{tv} + Y_{tv} + Z_{tv}} 100 \quad (17)$$

$$V_{fy} = \frac{Y_{tv}}{X_{tv} + Y_{tv} + Z_{tv}} 100 \quad (18)$$

$$V_{fz} = \frac{Z_{tv}}{X_{tv} + Y_{tv} + Z_{tv}} 100 \quad (19)$$

Table 3 - Weaver and manufacturer provided data for Carbon-Carbon-Carbon

	ṅ	**λ**	**n**	**Ƞ(g/km3)**	**ρ(kg/m3)**	**Pf**	**AR**
Stuffer S)	5	5	5	0.0002	1780	0.7854	1
Filler(F)	5	5	5	0.0002	1780	0.7854	1
Binder(B)	5	5	5	0.0002	1780	0.7854	1

Table 4 - Weaver and manufacturer provided data for Carbon-Carbon-Kevlar

	ṅ	**λ**	**n**	**Ƞ(g/km^3)**	**ρ(kg/m^3)**	**P_f**	**AR**
Stuffer(S)	5	5	5	0.0002	1780	0.7854	1
Filler(F)	5	5	5	0.0002	1780	0.7854	1
Binder(B)	5	5	5	0.000158	1450	0.7854	1

Table 5 - Weaver and manufacturer provided data for Kevlar-Kevlar-Carbon

	ṅ	λ	n	Ŋ(g/km^3)	ρ(kg/m^3)	P_f	AR
Stuffe (S)	5	5	5	0.000158	1450	0.7854	1
Filler(F)	5	5	5	0.000158	1450	0.7854	1
Binder(B)	5	5	5	0.0002	1780	0.7854	1

Table 6 - Weaver and manufacturer provided data for Kevlar-Kevlar-Kevlar

	ṅ	λ	n	Ŋ(g/km^3)	ρ(kg/m^3)	P_f	AR
Stuffer(S)	5	5	5	0.000158	1450	0.7854	1
Filler(F)	5	5	5	0.000158	1450	0.7854	1
Binder(B)	5	5	5	0.000158	1450	0.7854	1

2.4 Tensile Test

The goal is to determine the tensile strength, modulus of elasticity & Poisson's ratio. Measure the dimensions of the specimen and mark the gauge length. Insert the specimen into grips as shown in Fig.9. Apply load and record load v/s displacement data. Till a fracture happens, keep testing. [13] Measure the specimen's ultimate length and area by fusing the specimen's two fractured pieces together as indicated in Fig.14.

3. Result and Discussion

3.1 Analytical Calculations

The greatest force that a composite material can bear under a uniaxial load is defined as its tensile strength. Data on tensile strength, modulus, and strain-to-failure were acquired from testing ten specimens of each weave structure. The specimens were all submitted to rigorous testing, and it was discovered that the stress and strain had a proportionate connection in each case. No obvious plastic deformation was seen during the testing. At the maximum stress value, the testing was terminated so that the failed specimens could be inspected, and the causes of each failure could be determined. Following are the results obtained from analytical models and the thickness of two of the four variants is as follows, Tables 7, 8, 9, and 10. The thickness of unit cell of the four variants is shown in Table 11. Area, Length and volume of stuffer, filler and binder are calculated, of the four variants is as follow Tables 12-15. The binder tow's vertical component is shown in Table 16. Stuffers volume, in addition to the horizontal component of the binder, makes up the real volume of the tow shown in Table 17, whereas only the vertical component of the binder tows in the x and z directions are employed. The calculation of volume fraction Table 18.

Fig. 9 - UTM (BISS- Instron) - tensile test

Table 7 - Tow thickness of Carbon-Carbon-Carbon

CCC	T(m)
Stuffer	4.269e-04
Filler	4.269e-04
Binder	4.269e-04

Table 8 - Tow thickness of Carbon-Carbon-Kevlar

CCK	T(m)
Stuffer	4.269e-04
Filler	4.269e-04
Binder	4.204e-04

Table 9 - Tow thickness of Kevlar-Kevlar-Carbon

KKC	T(m)
Stuffer	4.204e-04
Filler	4.204e-04
Binder	4.269e-04

Table 10 - Tow thickness of Kevlar-Kevlar-Kevlar

KKK	T(m)
Stuffer	4.204e-04
Filler	4.204e-04
Binder	4.204e-04

Table 11 - Unit cell thickness

Type	T (m)
CCC	4.269e-03
CCK	4.269e-03
KKC	4.204e-03
KKK	4.204e-03

Table 12 - Yarn spatial properties of Carbon-Carbon-Carbon

	A (m^2)	L(m)	l (m)	V(m^3)
Stuffer	1.43e-07	62.5	2.5	8.94e-06
Filler	1.43e-07	62.5	2.5	8.94e-06
Binder	1.43e-07	0.2675	0.0107	3.8e-08

Table 13 - Yarn spatial properties of Carbon-Carbon-Kevlar

	A (m^2)	L(m)	l (m)	V(m^3)
Stuffer	1.43e-07	62.5	2.5	8.94e-06
Filler	1.43e-07	62.5	2.5	8.94e-06
Binder	1.38e-07	0.2667	0.01067	3.128e-08

Table 14 - Yarn spatial properties of Kevlar-Kevlar-Carbon

	A (m^2)	L(m)	l (m)	V(m^3)
Stuffer	1.38e-07	62.5	2.5	8.66e-06
Filler	1.38e-07	62.5	2.5	8.66e-06
Binder	1.38e-07	0.2627	0.01051	3.64e-08

Table 15 - Yarn spatial properties of Kevlar-Kevlar-Kevlar

	A (m^2)	L(m)	l (m)	V(m^3)
Stuffer	1.38e-07	62.5	2.5	8.62e-06
Filler	1.38e-07	62.5	2.5	8.62e-06
Binder	1.43e-07	0.2625	0.0105	3.75e-08

Table 16 - Binder tow vertical component

Type	Z (m)
CCC	0.04269
CCK	0.04269
KKC	0.04204
KKK	0.04204

Table 17 - Tow volume

TYPE FOR	X	Y	Z
CCC	8.97e-06	8.94e-06	6.1e-09
CCK	8.97e-06	8.94e-06	6.47 e-10
KKC	8.65e-06	8.62e-06	6.34e-10
KKK	8.68e-06	8.66e-06	5.83e-09

Table 18 - Volume fractions

Volume Fraction Vf			
TYPE	**X**	**Y**	**Z**
CCC	50.06	49.89	0.034
CCK	50.08	49.9	0.02
KKC	50.06	49.89	0.034
KKK	49.89	49.89	0.209

Table 19 - Elastic constants

CCC	**E(GPa)**
X	121.84
Y	121.43
Z	3.48
CCK	**E(GPa)**
X	121.89
Y	121.46
Z	3.42
KKC	**E(GPa)**
X	57.76
Y	57.58
Z	3.48
KKK	**E(GPa)**
X	57.58
Y	57.58
Z	3.63

3.2 Experimental Results

Fig.10–13. of the accompanying graphs and data show that carbon–carbon–carbon plates have greater tensile strength than the other plates. Noticed that the combination of CCK and KKC have nearby values. As proved that Kevlar fabric can withhold higher impact strength than tensile strength, Fig. 11. The tensile test specimens are shown in Fig.14 and the average peak stress is shown in Table 20. Inside structures of the 3Dcarbon composites are shown in Figures 15(a, b) below are the SEM images in wrap direction, weft direction and top view. Here we observe matrix accumulation below the Z-binder, void, and Z- binder. A potential weakness in the 3D structure is when the binding tow enters the fabric layers to complete the binding. Weakness in this section of the composite has been linked to resin build-up caused by weft tow collimation and binder tow pinching as they pass through the structure.

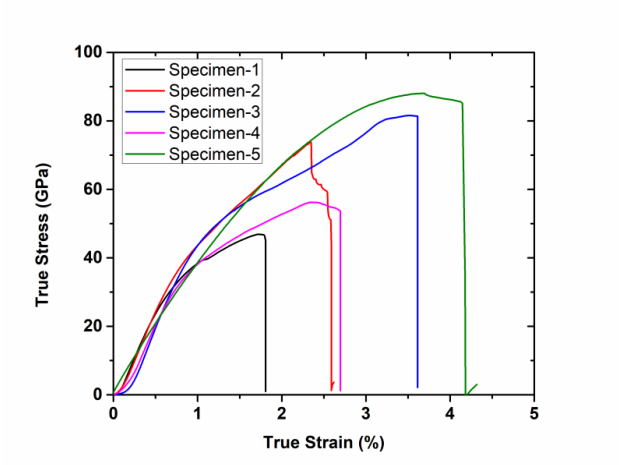

Fig.10 - Stress vs strain for C-C-C

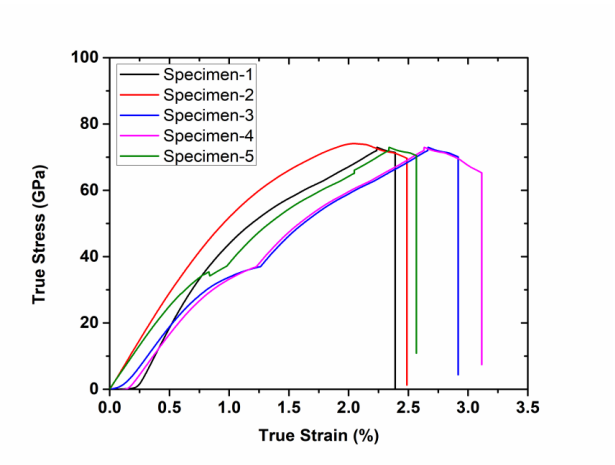

Fig. 11 - Stress vs strain for C-C-K

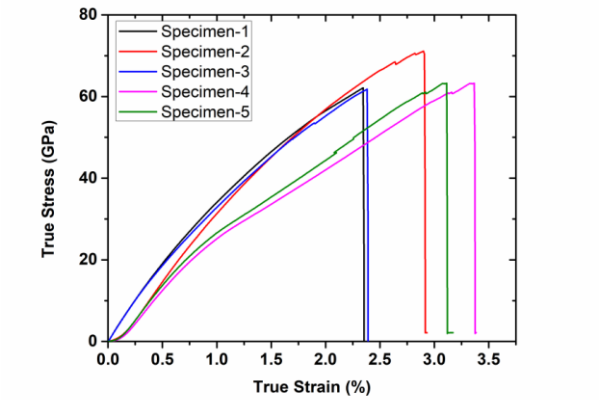

Fig. 12 - Stress vs strain for K-K-C

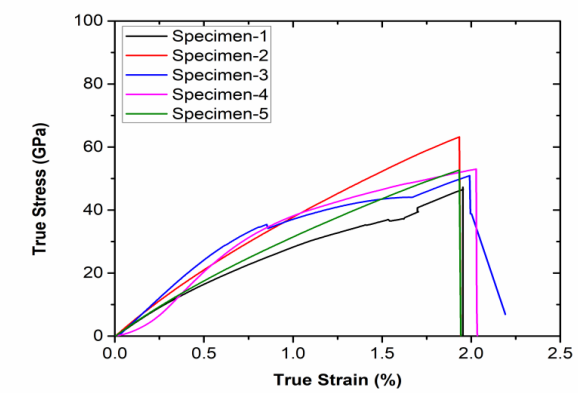

Fig. 13 - Stress vs strain for K-K-K

Fig. 14 - Tested samples

Table 20 - Tensile test result

Specimen	Average Peak Stress (Mpa)	Weight (Gms)	Strength To Weight Ratio
CCC	88	62	1.41
CCK	60.6	60	1.01
KKC	60.2	58	1.03
KKK	30.2	55	0.54

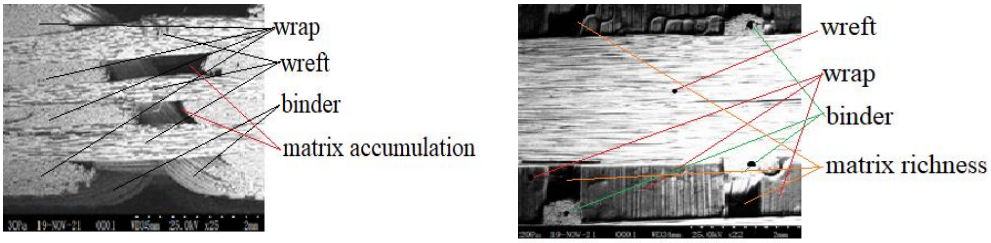

(a) (b)

Fig. 15 - SEM showing wreft, wrap, binder, and matrix (a) side view; (b) top view

4. Conclusion

Four distinct types of 3D woven composites have been explored, and an overview of the analytical modelling, modelling of the mesoscale geometry, elastic constants, and experimental data has been done. Drew attention to the 3D woven composite research's areas of a higher strain. Carbon fibres were woven into plates in both the weft and warp directions, giving them a tensile strength superior to Kevlar. Comparing the 3D woven composite to the 2D plain weave plied lay-up, the tensile strength is somewhat lower. The decrease in tensile strength is thought to occur for a variety of causes, including:

i. The effectiveness of the structure was lowered by crimp caused by the binder tows added during the weaving process.
ii. By collimating the weft threads, which happens because of uncontrolled binder tow tension, resin-rich regions are produced.
iii. As the binder tow went into and out the fabric, it sheared.
iv. Large binders led resin-rich regions around the binder to spin, resulting in areas of intense strain. However, the data pattern provides critical information on the characteristics of the composite material under tensile loading.
v. The magnitude of the strain figures provided by these tests requires further verification. This was an expected outcome because carbon has a greater modulus for Young's modulus.
vi. The test results were as expected, and this will open new doors for further studies in this area.

Some of them are, a faster and more efficient method of weaving can be developed because hand weaving is very inconsistent and causes a lot of fiber breaks, the analytical models present right now can also be improved for more accurate outcomes.

Acknowledgement

The authors appreciate and recognize the support rendered by the staff of Composite Materials laboratory, Material Testing Laboratory and Simulation Laboratory, HITS, Chennai and NMIT, Bangalore for permitting to use of their facilities for study, data collection and analysis.

References

[1] Piergiorgio Valentino, Emanuele Sgambitterra, Franco Furgiuele “Mechanical characterization of basalt woven fabric composites: numerical and experimental investigation” [2014]
[2] Owais Anwar Golraa, Jawad Tariqb, Nadeem Ehsanc and Ebtisam Mirzad, “Strategy for introducing 3D fibre reinforced composites weaving technology” [2012]
[3] Xiaogang. Chen, Lindsay. W. Taylor and Li. Ju Tsai, “An Overview on Fabrication of three-dimensional woven textile preforms for composites” [2011]
[4] Yoshiyuki Kobayashi, Makoto Ito “Development of 3-D woven composites for aircraft structures” [2009]
[5] Hassan M. El-Dessouky and Mohamed N. Saleh [2018]
[6] P. Gurkan, “3D Woven Fabrics,” Woven Fabr., no. May, 2012, doi: 10.5772/37492.
[7] L. Jin, Z. Niu, B. C. Jin, B. Sun, and B. Gu, “Comparisons of static bending and fatigue damage between 3D angle-interlock and 3D orthogonal woven composites,” J. Reinf. Plast. Compos., vol. 31, no. 14, pp. 935–945, 2012, doi: 10.1177/0731684412450626.
[8] E. Archer, S. Buchanan, A. McIlhagger, and J. Quinn, “The effect of 3D weaving and consolidation on carbon fiber tows, fabrics, and composites,” J. Reinf. Plast. Compos., vol. 29, no. 20, pp. 3162–3170, 2010, doi: 10.1177/0731684410371405.
[9] M. N. Saleh and C. Soutis, “Recent advancements in mechanical characterisation of 3D woven composites,” Mech. Adv. Mater. Mod. Process., vol. 3, no. 1, 2017, doi: 10.1186/s40759-017-0027-z.
[10] J. Huang et al., “Effect of microcracks on the tensile properties of 3d woven composites,” Coatings, vol. 11, no. 7, pp. 1–15, 2021, doi: 10.3390/coatings11070794.

[11] M. Ansar, W. Xinwei, and Z. Chouwei, "Modeling strategies of 3D woven composites: A review," Compos. Struct., vol. 93, no. 8, pp. 1947–1963, 2011, doi: 10.1016/j.compstruct.2011.03.010.
[12] J. Cao et al., "Characterization of mechanical behavior of woven fabrics: Experimental methods and benchmark results," Compos. Part A Appl. Sci. Manuf., vol. 39, no. 6, pp. 1037–1053, 2008, doi: 10.1016/j.compositesa.2008.02.016.
[13] B. N. Cox, M. S. Dadkhah, and W. L. Morris, "On the tensile failure of 3D woven composites," Compos. Part A Appl. Sci. Manuf., vol. 27, no. 6, pp. 447–458, 1996, doi: 10.1016/1359-835X(95)00053-5.
[14] D. Abe, O. Bacarreza, and M. H. Aliabadi, "Micromechanical modeling for the evaluation of elastic moduli of woven composites," Key Eng. Mater., vol. 525–526, pp. 73–76, 2012, doi: 10.4028/www.scientific.net/KEM.525-526.73.
[15] S. Z. H. Shah, P. S. M. Megat Yusoff, S. Karuppanan, and Z. Sajid, "Elastic constants prediction of 3d fiber-reinforced composites using multiscale homogenization," Processes, vol. 8, no. 6, pp. 1–12, 2020, doi: 10.3390/pr8060722.
[16] D. P. C. Aiman, M. F. Yahya, and J. Salleh, "Impact properties of 2D and 3D woven composites: A review," AIP Conf. Proc., vol. 1774, 2016, doi: 10.1063/1.4965050.
[17] A. K. Bandaru, S. Patel, Y. Sachan, R. Alagirusamy, N. Bhatnagar, and S. Ahmad, "Low velocity impact response of 3D angle-interlock Kevlar/basalt reinforced polypropylene composites," Mater. Des., vol. 105, pp. 323–332, 2016, doi: 10.1016/j.matdes.2016.05.075.
[18] Z. gui Li, D. sen Li, H. Zhu, Z. xin Guo, and L. Jiang, "Mechanical properties prediction of 3D angle-interlock woven composites by finite element modeling method," Mater. Today Commun., vol. 22, p. 100769, 2020, doi: 10.1016/j.mtcomm.2019.100769.